Proceedings of GT2008
ASME Turbo Expo 2008: Power for Land, Sea and Air
June 9-13, 2008, Berlin, Germany

GT2008-50322

Overspray and Interstage Fog Cooling in Compressor Using Stage-Stacking Scheme – Part 1: Development of Theory and Algorithm

Ting Wang and Jobaidur R. Khan
Energy Conversion & Conservation Center
University of New Orleans
New Orleans, LA 70148-2220, USA

ABSTRACT

Compressor intercooling has traditionally been employed to reduce compressor work and augment gas turbine output power. Conventional intercooling schemes are usually applied through non-mixed heat exchangers between two compressor stages or by cooling the outside of the compressor casing. Any cooling schemes that may affect the flow field inside the compressors have not been favorably considered due to concerns of any disturbance that might adversely affect the compressor's performance stability. As the inlet fog cooling scheme has become popular as an economic and effective means to augment gas turbine output power on hot or dry days, consideration has been given to applying fog cooling inside the compressors by injecting fine water droplets between stages (i.e. interstage fogging). This paper focuses on developing a stage-by-stage wet-compression theory for overspray and interstage fogging that includes the analysis and effect of pre-heating and pre-cooling at each small stage of the overall compressor performance. An algorithm has been developed to calculate the local velocity diagram and allow a stage-by-stage analysis of the fogging effect on airfoil aerodynamics and loading with known 2-D meanline rotor and stator geometries. Thermal equilibrium model for water droplet evaporation is adopted. The developed theory and algorithm are integrated into the system-wise FogGT program to calculate the overall gas turbine system performance.

NOMENCLATURE

C_P	Specific Heat at Constant Pressure (kJ/kg-K)
dm	Evaporated differential mass
E	Evaporation rate
f	Fraction of liquid water
g	Fraction of water vapor
h	Static Enthalpy (kJ/kg)
ho	Total Enthalpy (kJ/kg)
k	Polytropic index
L	Latent heat of water (kJ/kg)
M	Molecular weight (kg/kmole)
Ma	Mach number
$\dot{m}$	Mass flow rate (kg/s)
P	Pressure (kPa)
P_o	Total pressure (kPa)
r	Mean radius
R	Gas constant (kJ/kg-K)
R_0	Universal gas constant (8.314 kJ/kmole-K)
RH	Relative humidity
r_p	Overall pressure ratio
s	Fraction of superheated steam
SF	Shape factor
T	Temperature (K)
T_o	Total Temperature (K)
Tq	Torque (Nm)
U	Tangential velocity
v	Specific volume (m^3/kg)
V	Inlet velocity
V_a	Axial velocity
V_u	Projected velocity
Work	Work (kJ)
W	Relative velocity

Greek

γ	Specific heat ratio (c_p/c_v)
η_C	Overall compressor efficiency
η_p	Polytropic (or small-stage) efficiency
η_S	Isentropic stage efficiency
ρ	Density (kg/m^3)

Subscripts

1, 2,..	Stage numbers
a	Dry air fraction
amb	Ambient
D	Design point
Dry	Dry compression
f	Liquid water fraction
g	water vapor fraction
i	Rotor Stage
i+0.5	Stator Stage
s	Superheated steam fraction
S	Isentropic process

INTRODUCTION

Compressor intercooling has traditionally been employed to reduce compressor work and augment gas turbine output power. Conventional intercooling schemes are usually applied through non-mixed heat exchangers between two compressor stages or by cooling the outside of the compressor casing. Any cooling schemes that may affect the flow field inside the compressors have not been favorably considered by industry due to concerns of any disturbance that might damage compressor airfoils or adversely affect the compressor's performance stability. As the inlet fog cooling scheme has become popular as an economic and effective means to augment gas turbine output power on hot or dry days [1], consideration has been given to applying overspray (high) fog cooling or injecting fine water droplets between stages (i.e. interstage fogging). There are several concerns associated with overspray or interstage water spray cooling: (a) the potential erosion of compressor blades caused by tiny water droplets, (b) drilling holes through the compressor casings to install fogging devices may cause a compressor integrity problem, (c) the manufacturer's warranty could be voided. Furthermore, Bagnoli et. al. [2] has shown that more power can be obtained by applying fogging upstream of the compressor than between the stages. Therefore, overspray or interstage fogging has not been widely applied and is still subject to further research and investigation.

Irrespective of the above concerns, there are several other reasons for implementing interstage fogging. Ingistov [3] pointed out that a water injection system was installed in a 7EA gas turbine to wash the compressor blades and preserve the gas turbine output power rather than augment power output. Shepherd and Fraser [4] presented field data from a Siemens gas turbine to compare the performance between applying inlet and interstage fogging. The data showed that output power augmentation obtained by applying the interstage fogging is almost insensitive to the ambient temperature variation. They treated this feature as a merit of interstage fogging. The data further showed NOx reduction was more pronounced by applying interstage fogging than inlet cooling. They also mentioned the risk associated with spraying water into a compressor such as issues related to water distribution, degradation of compressor inlet duct materials, fouling of the compressor, compressor casing distortion, disturbance to the combustion dynamic pressure, and the need to tune the control system integration.

Wet Compression

Thermodynamic wet compression model was established by Hill [5] and was further developed by Zheng et al. [6&7]. Their analysis provided the relationship between the dry compression index and wet compression index. Ransom et. al. [8] showed calculation procedure of enthalpy and some of the limitations of its calculation with associated source of errors.

Using aero-thermodynamic modeling, Bagnoli et. al. [2] investigated the effects of interstage water injection on the performance of a 17-stage gas turbine. Moreover, to estimate the overall gas turbine performance, they discussed the impact of interstage injection by viewing the stage-by-stage compressor performance of selected gas turbines. They found better power augmentation could be obtained if the water injection is applied upstream of the compressor compared to other injection locations between stages. Since the maximum amount of water injection is limited by ambient conditions, maximum allowable gas turbine power output and the compressor surge limit, they cautioned that increasing the amount of water injection may cause the last compressor stage to operate closer to the surge line. This is in contrast to the conclusion made by Li and Zheng [9], who conducted a stability analysis and stated that injection of water mist can stabilize the compressor and delay surge and rolling stall. At this point, which statement is correct is not known until more tests can be performed. Roumeliotis et al. [10] studied both inlet and interstage water injection on compressor stall margin. Their results indicated that the stall margin diminished with both inlet and interstage water injection due to a change of compressor operation point and a simultaneously movement of surge line towards lower pressure ratios, which were in agreement with the information presented by Lecheler et. al. [11].

Payne and White [12] presented the calculation procedure for evaporative flow of three-dimensional blade rows. However, they only analyzed the injection of small droplets which were assumed to follow the main flow. Their results showed that the main change occurs due to the reduction of axial velocity and evaporation. As a result, blade pressure distribution changed. They acknowledged that further work is required to include all the effects of velocity slip relevant to larger droplets.

Bagnoli et. al. [13] developed a calculation code by modeling the exchange of latent heat at the inlet and outlet stage as well as the exchange of sensible heat at constant temperature and pressure in the middle of the stage. Using the model developed above, Bagnoli et. al. [14] investigated the effects of interstage water injection on the performance of a GE Frame 7EA gas turbine. They found that gas turbines lost approximately 15% power output due to high ambient temperature compared to the ISO case. 1.6% of water injection at stator of the compressor stage #2 allows recovery of the lost power for high ambient temperature. They also found that the power boost per unit of water injection decreases as the injection point moves from the first to the fifth stage. The droplet residence time decreases as the injection point moves closer to the compressor inlet. In the case of water injection, the maximum reduction in compressor specific work (that reaches a value of about 97% of the specific work in ISO dry case), takes place with injecting in the inlet duct at high ambient temperature conditions. White and Meacock [15] described the method of meanline calculation for wet compression. They applied the method to see the nature of the off-design condition due to evaporative cooling. In their calculation, they assumed that the polytropic efficiency is not affected by evaporation and the entropy changes due to irreversible phase change has been taken into consideration using an equation provided by Young..

Abdelwahab [16] applied the wet compression to a centrifugal compressor. He found that small droplet radii lead to a much faster evaporation time compared to the fluid particle travel time. The higher the injection rate, the higher the total pressure ratio the stage can develop. This is due to colder compression temperatures allowing the work transferred from the impeller to the flow and then converted into higher total pressures. This fact is also true for axial flow gas turbines and was shown by Zamzam and Al-Amiri [17] that cooled denser air gives the system a higher mass flow rate and pressure ratio, resulting in an increase in combustion turbine output.

Sanaye et. Al. [18] studied the effects of inlet fogging and wet compression on gas turbine performance. They modeled the evaporation of water droplets in the compressor inlet duct and estimated the diameter of water droplets at end of the inlet duct. They compared their findings with the results from FLUENT software. They also predicted the compressor discharge air temperature due to the presence of unevaporated water at the inlet duct. They found that flow coefficient increases in first few stages due to the water spray. This leads to the increase in axial velocity at the first few stages and the corrected speed increases due to the

cooling of compressor inlet air. The result showed an increase in density and pressure and a decrease in the axial velocity at later compressor stages. The amount of water injection increases with increasing pressure ratio. Following the work of Spina [19], they employed the generalized compressor performance curve to calculate the rotor work coefficient of each stage and applied the method to GE9171E.

Bianchi et. al. [20] studied the influence of water droplet size and temperature of wet compression in a 17-stage compressor. They concluded that the gas turbine performance improves for finer and hotter droplets, as does the evaporation velocity. They also found that the redistribution of compressor stages load, which means an unloading of the first compressor stages and an overloading of the last compressor stages, is influenced by the injection diameter and temperature of liquid water droplets. Their analysis did not consider the cost of preheating water to produce hotter droplets. Sexton et. al. [21] conducted a simulation on suppressing NO_x by employing evaporative compressor cooling. The results show that the compressor performance maps (in terms of shaft power, pressure ratio, efficiency etc.) were changed due to wet compression. They assumed that the evaporation rate depends on the mass diffusion and each droplet travels with no slip with air. They assumed all the stages were frictionless and adiabatic.

Kim and Perez-Blanco [22] explained the theoretical limits of machines via a heat and mass transfer model and modeled continuous compression cooling via evaporation numerically based on droplet evaporation analysis. They found, initially, the increase of the droplet temperature overrides the decrease in droplet mass and results in an internal energy increase in the droplet. The internal energy peaks and then decreases with time as the liquid evaporates.

Khan and Wang [23] developed a wet compression thermodynamic model for a gas turbine system (FogGT) with inlet fog cooling specifically for burning low calorific value (LCV) fuels. The results showed that in the combustor, as heating value decreases for LCV fuels, there are more incombustible gases in the fuel to absorb the energy and suppress the combustion temperature; so more heat addition (23%-46%) is required to allow the combusted gas to reach the desired TIT. In the turbine, the LCV fuels produce more net output power than natural gas, even though LCV fuels significantly increase fuel compressor power. When LCV fuels are burned, saturated fogging can achieve a net output power increases approximately 1-2%, while 2% overspray can achieve 20% net output enhancement. As the ambient temperature or relative humidity increases, the net output power decreases. For LCV fuels, the thermal efficiency is approximately 10~16% (3~5 percentage points) lower than using natural gas. Burning LCV fuel leads to small changes in thermal efficiency irrespective of a large increase in net power output because the increased demand for additional heat input makes up the sensible heat required for increased fuel flow rate including incombustible gases. Fog/overspray could either slightly increase or decrease the thermal efficiency depending on the ambient conditions.

Compressor Generalized Performance Curves

During the development of the wet compression model, one roadblock was the unavailability of the compressor performance map because it has been guarded by the gas turbine manufacturers as proprietary information. To overcome this problem, Spina [19] summarized the method of using generalized performance curves of compressors and turbines. In using the generalized performance curves, a Shape Factor (SF) needs to be determined to help the blade loading (work coefficient) and flow coefficient or each stage subject to wet compression. Almost all the previous non-CFD analytical studies [9, 12-16] employed the scheme of generalized performance curves. Unfortunately, the selection of the SF is also an uncertain process. Not much has been published in the literature to discuss how to reduce this uncertainty. In view of the aforementioned issues and to avoid using the generalized performance curves, the **objective** of this paper is two fold: (a) employ a **stage-stacking** approach by developing a stage-by-stage wet-compression analysis using 2D compressor airfoil geometries and stage settings at the mean radii of the airfoils and (b) use the stage-stacking results to calculate the SF values to asses the potential improvement for using the generalized compressor performance curve to study wet compression. The thermodynamic analysis for interstage fogging includes the pre-heat and pre-cool effect at each small stage on the overall compressor performance. Following this approach, the elemental stage polytropic efficiency can be kept constant throughout the compressor. This approach provides actual aero-thermal interactions with the velocity triangular diagram and especially the performance of each stage where interstage fogging can be calculated. Thermal equilibrium model is adopted.

THERMODYNAMIC MODEL

Consider an axial flow compressor consisting of a number of successing stages. The difference between the single-stage efficiency, $\eta_{c,single}$,, and the overall compressor efficiency, $\eta_{c,}$ increases as compression ratio increases. The increase in temperature, due to reversible compression as well as irreversible friction in one-stage, result in more work being required in the next stage. The effect is termed "**preheat** effect" by Saravanamuttoo et. al. [24] This phenomenon has led to the concept of "small-stage efficiency" (or polytropic efficiency, η_p), which is defined as the isentropic efficiency of an elemental (or differential) stage in the process such that the pressure ratio approaches the limit of unity. This can be done mathematically by adding a perturbation term to the pressure ratio, expanding the isentropic efficiency around the pressure ratio with binomial theorem, and taking the limit of perturbation term towards zero [25]. This will give the small-stage efficiency, which will not change during the compressing process at the same operating condition. During interstage fogging, an opposite process occurs at each elemental stage due to evaporative cooling of tiny water droplets. Employing the same concept as the "preheat small-stage efficiency," a "**precool small stage**" approach is adopted in the analysis used in this paper. The merit of this approach is that the referenced polytropic efficiency of an elemental (or differential) stage can be treated constant throughout the entire process, irrespective of the local temperature and pressure when the blade row design is similar in successive stages [19 and 25]. It needs to be noted that if the wet compression affects the operating condition, the small-stage efficiency could change at different stages due to the shift of operating point.

Preheat and Precool Effect of Small Stage

In Fig 1, the T-s diagram shows the elemental stages and their thermodynamic behavior of the air. 1-2s, 2s-3s, and 3s-4s show the ideal dry compression in the 1st, 2nd and 3rd stages. 1-2a, 2a-3a, and 3a-4a show the actual dry compression in 1st, 2nd and 3rd stages. It is clear in the figure that T_{2a} is higher than $T_{2S,}$ where this higher temperature preheats the second stage. Similarly T_{3a} preheats the third stage and so on. Since the isobaric lines diverge on the T-s diagram, the vertical distance between two isobars lines increases at higher entropy values; so even if each differential stage compresses

isentropically, the preheat effect will degrade the overall compressor efficiency.

During an interstage fogging application, for example, if water mist is sprayed in the second stage, evaporation takes place and the temperature at the end of the second stage (or the beginning of the third stage) will be reduced to T_{3w} from T_{3a}. T_{3w} could be lower or higher than $T_{3s'}$, which corresponds to the isentropic process starting at T_{2a}. If T_{3w} is higher than $T_{3s'}$, the preheat effect on stage 3 is reduced; if T_{3w} is lower than $T_{3s'}$, stage 3 is precooled. It should be noted that the evaporation process is irreversible and nonisentropic; however, it can be represented as a cooling process of air with a nonisentropic polytropic index k (not γ, which is the mixture's specific heat ratio.)

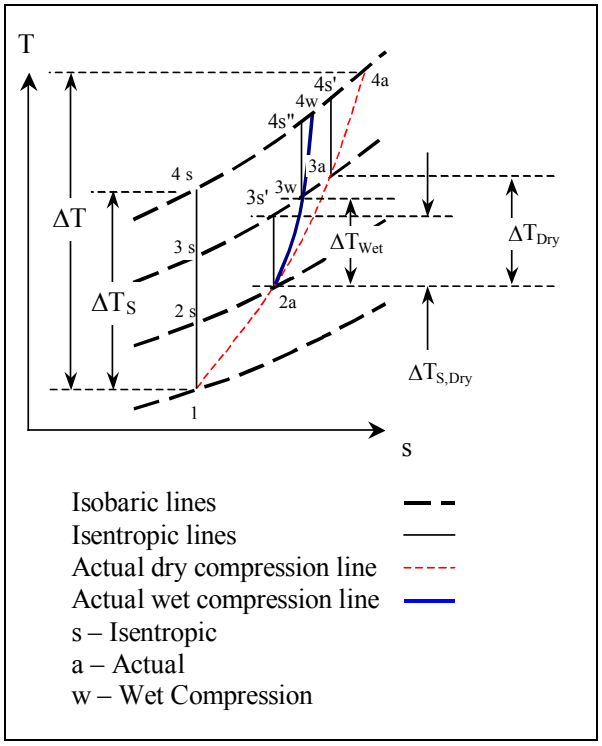

Figure 1 Pre-heat and pre-cool effect on air due to evaporative cooling. This figure only qualitatively represents the behavior of the air, but not the complete wet compression process.

For an ideal wet compression process [5],

$$\frac{dP}{P} = \left(\frac{\gamma}{\gamma - 1} + \frac{L}{R}\frac{dm}{dT}\right)\frac{dT_S}{T} \qquad (1)$$

Integrating Eq. (1) between stage 1 and stage 2, we get,

$$\frac{T_{2S}}{T_1} = \left(\frac{P_2}{P_1}\right)^{1\Big/\left(\frac{\gamma}{\gamma-1}+\frac{L}{R}\frac{dm}{dT}\right)} \qquad (2)$$

Efficiency for the differential stage 1 and 2,

$$\eta_{St} = \frac{\left(m_{a_{1+dS}} h_a\big|_{T_1+dT_s} - m_{a_1} h_a\big|_{T_1}\right) + \left(m_{f_{1+dS}} h_f\big|_{T_1+dT_s} - m_{f_1} h_f\big|_{T_1}\right) + \left(m_{g_{1+dS}} h_g\big|_{T_1+dT_s} - m_{g_1} h_{g_1}\right)}{\left(m_{a_{1+d}} h_a\big|_{T_1+dT} - m_{a_1} h_a\big|_{T_1}\right) + \left(m_{f_{1+d}} h_f\big|_{T_1+dT} - m_{f_1} h_f\big|_{T_1}\right) + \left(m_{g_{1+d}} h_g\big|_{T_1+dT} - m_{g_1} h_{g_1}\right)} \qquad (3)$$

where, $m_{f_{1+d}} = m_{f_1} - dm$ and $m_{g_{1+d}} = m_{g_1} + dm$

and, $m_{f_{1+dS}} = m_{f_1} - dm_S$ and $m_{g_{1+dS}} = m_{g_1} + dm_S$

Where, dm = Evaporated amount of water to water vapor

As the amount of dry air remains same, so,

$$m_{a_{1+d}} = m_{a_{1+dS}} = m_{a_1} = m_a$$

Put these values into Eq. (3), the differential stage efficiency becomes,

$$\eta_P = \frac{m_a\left(h_a\big|_{T_1+dT_s} - h_a\big|_{T_1}\right) + m_{f_1}\left(h_f\big|_{T_1+dT_s} - h_f\big|_{T_1}\right) + m_{g_1}\left(h_g\big|_{T_1+dT_s} - h_g\big|_{T_1}\right) + L_{T_1+dT_s} dm_S}{m_a\left(h_a\big|_{T_1+dT} - h_a\big|_{T_1}\right) + m_{f_1}\left(h_f\big|_{T_1+dT} - h_f\big|_{T_1}\right) + m_{g_1}\left(h_g\big|_{T_1+dT} - h_g\big|_{T_1}\right) + L_{T_1+dT} dm}$$

$$\Rightarrow \eta_P = \frac{m_a Cp_a + m_{f_1} Cp_f + m_{g_1} Cp_g + L_{T_1+dT_s}\dfrac{dm_S}{dT_S}\dfrac{dT_S}{dT}}{m_a Cp_a + m_{f_1} Cp_f + m_{g_1} Cp_g + L_{T_1+dT}\dfrac{dm}{dT}} \qquad (4)$$

Here, $\frac{dm}{dT}$ is the evaporation rate which is assumed the same as the evaporation rate in the isentropic process. This assumption is based on the reasoning that even though the actual evaporated water mass and the temperature change during evaporation are different between the actual and isentropic processes, their ratios (dm/dT and dm_s/dT_s), ie. the evaporation rates, are approximately the same. So

$$\frac{dm}{dT} = \frac{dm_S}{dT_S} = E$$

The latent heat, L, is a function of temperature. Take the first-order approximation

$$L_{T_1+dT} = L(T_1 + dT) = L(T_1) + L'(T_1)dT$$

$$L_{T_1+dT_S} = L(T_1 + dT_S) = L(T_1) + L'_S(T_1)dT_S$$

In the numerator and denominator of Eq. (4), the first three terms and the zeroth order term of the Taylor's expansion are constant because the inlet condition is fixed, so

$$m_a Cp_a + m_{f_1} Cp_f + m_{g_1} Cp_g + L(T_1) = K$$

Eq. (4) becomes,

$$\eta_p = \frac{K + L'_S(T_1)EdT_S}{K + L'(T_1)EdT}\frac{dT_S}{dT}$$

$$\Rightarrow \qquad \eta_p = \frac{KdT_S + L'_S(T_1)E(dT_S)^2}{KdT + L'(T_1)E(dT)^2}$$

[Neglect higher order (e.g. dT^2) terms]

$$\Rightarrow \qquad \eta_p = \frac{KdT_S}{KdT} = \frac{dT_S}{dT}$$

$$\Rightarrow \qquad \frac{T_2}{T_1} = \left(\frac{P_2}{P_1}\right)^{1/\left[\eta_p\left(\frac{\gamma}{\gamma-1}+\frac{L}{R}E\right)\right]} \qquad (5)$$

The stage isentropic efficiency is

$$\eta_S = \frac{\left(m_{a_{2S}} h_{a_{2S}} - m_{a_1} h_{a_1}\right) + \left(m_{f_{2S}} h_{f_{2S}} - m_{f_1} h_{f_1}\right) + \left(m_{g_{2S}} h_{g_{2S}} - m_{g_1} h_{g_1}\right)}{\left(m_{a_2} h_{a_2} - m_{a_1} h_{a_1}\right) + \left(m_{f_2} h_{f_2} - m_{f_1} h_{f_1}\right) + \left(m_{g_2} h_{g_2} - m_{g_1} h_{g_1}\right)} \qquad (6)$$

Here, $m_{f_2} = m_{f_1} - m$ and $m_{g_2} = m_{g_1} + m$,

and, $m_{f_{2S}} = m_{f_1} - m_S$ and $m_{g_{2S}} = m_{g_1} + m_S$

Where, m = Evaporated amount of water to water vapor

As the amount of dry air remains same, so,

$m_{a_{2S}} = m_{a_2} = m_{a_1} = m_a$

$$\eta_S = \frac{\left(m_a C_{P_a} + m_{f_1} C_{P_f} + m_{g_1} C_{P_g} + EL_{2S}\right)\left(T_{2S} - T_1\right)}{\left(m_a C_{P_a} + m_{f_1} C_{P_f} + m_{g_1} C_{P_g} + EL_2\right)\left(T_2 - T_1\right)}$$

$$\Rightarrow \eta_S = \frac{\left(m_a C_{P_a} + m_{f_1} C_{P_f} + m_{g_1} C_{P_g} + EL_{2S}\right)\left[r_P^{1/\left(\frac{\gamma}{\gamma-1}+\frac{L\,dm}{R\,dT}\right)} - 1\right]}{\left(m_a C_{P_a} + m_{f_1} C_{P_f} + m_{g_1} C_{P_g} + EL_2\right)\left[r_P^{1/\left[\eta_P\left(\frac{\gamma}{\gamma-1}+\frac{L\,dm}{R\,dT}\right)\right]} - 1\right]} \qquad (7)$$

Eq. (7) shows the compressor isentropic stage efficiency as a function of the pressure ratio including the stage pre-heat and pre-cool effects. An equivalent polytropic index of an actual wet compression (k) can be calculated as [Zheng et. al. (6)]:

$$\frac{\gamma}{\gamma-1} + \frac{L}{R}\frac{dm}{dT} = \frac{k}{k-1} \qquad (8)$$

This relationship makes Eq. (7) as,

$$\eta_S = \frac{\left(m_a C_{P_a} + m_{f_1} C_{P_f} + m_{g_1} C_{P_g} + EL_{2S}\right)\left[r_P^{(k-1)/k} - 1\right]}{\left(m_a C_{P_a} + m_{f_1} C_{P_f} + m_{g_1} C_{P_g} + EL_2\right)\left[r_P^{(k-1)/k\eta_P} - 1\right]} \qquad (9)$$

Eq. (9) is the relationship of the stage isentropic efficiency, η_S, and the small-stage efficiency, η_p, in terms of the equivalent polytropic index (k) for the moist air. A further approximation can be made by assuming $L_2 \approx L_{2S}$ and extend Eq. (9) to cover the entire compressor. This will lead to an approximation of the overall compressor isentropic efficiency η_C (Eq. 10) in terms of the overall pressure ratio, equivalent polytropic index of moist air, and the small-stage efficiency.

$$\eta_C \approx \frac{r_P^{(k-1)/k} - 1}{r_P^{(k-1)/k\eta_P} - 1} \qquad (10)$$

Eq. (10) provides a quick estimation of compressor wet compression efficiency. It could introduce approximately 5 percentage point error in compressor efficiency by assuming $L_2 \approx L_{2S}$. Eq. 9 is used in the current study, but not Eq. 10. It needs to be reminded that the above equation employes the assumption that the polytropic efficiency does not change due to wet compression [15].

As mentioned in the Introduction, previous papers [9, 12-16] did not include the blades geometry and aerodynamics calculations; rather they used the generalized compressor performance curve and the guessed shape factors to estimate the airfoil's work load and aerodynamics performance. In contrast, this study employs the stage-stacking approach by developing a stage-by-stage wet-compression analysis using an actual 2D compressor airfoil geometry and stage settings at the mean radii of the airfoils. Similar approaches using meanline airfoil geometry were performed by [15, 21, and 26].

Numerical Algorithm for Stage Performance

First, the geometries of the airfoils (stator and rotor) and the stagger angle are selected. The compressor passage geometry is designed on the basis of ISO Condition (288K and 60% relative humidity).

In the design condition, the rotor absolute inlet flow at each stage is assigned with zero tangential velocity. The blade inlet angle is set equal to the air inlet angle. The detailed procedure and formulation for stage-to-stage wet compression is documented in the next section "Numerical Procedure in Details". A brief summary of the procedure is provided here:

In summary, the inlet condition at the first stage rotor is given as the static condition. The total (or stagnation) status is obtained by guessing a total temperature and iterating until the total enthalpy obtained by two different methods converge. The air-water mixture mass flow rate at the first rotor inlet is calculated by assuming the compressor functions with the constant-volume-flow characteristics at the inlet. At the rotor exit, the flow is assumed to be turned at the exact angle as the blade camber angle. The status at the rotor exit is determined by matching the exit mass flow rate with the mass flow at the inlet plus the interstage mist injection if any. Two unknowns, density and absolute axial flow velocity, need to be determined during this mass flow rate matching process; therefore, two iterating loops are required. The first iteration starts by guessing the absolute axial exit velocity and drawing the velocity diagram. Iterations are conducted to ensure specific stage work obtained from the velocity diagram matches the total enthalpy increase obtained from the polytropic relationship. This includes the preheat and precool effect with a constant small-stage efficiency. Using the stagnation status obtained by the first iteration loop, the second iteration calculates the air-water mixture density and goes back to the first loop until the mass conservation is satisfied.

The procedure for determining the second or later rotor inlet condition is different from determining the first rotor inlet status. Instead, the total status at the later stage rotor inlet is known, and the static status needs to be determined. The procedure for determining the rotor exit condition is the same for all stages.

The effect of inlet or interstage fogging will change the flow coefficient and the flow inlet angle, which in turn will affect the pressure ratio and specific work of each stage.

Assumptions

1. Constant inlet axial velocity (or inlet flow coefficient) -- The compressor is assumed to behave as a constant-volume-flow-rate device at the inlet when the rotating speed is fixed, so the inlet axial velocity maintains constant. When fogging is applied, the volume flow rate at the inlet does not change although the mass flow rate increases due to increased air density. Therefore, it is important to realize that the inlet velocity maintaining a constant does not mean the mass flow rate maintains constant at the inlet. Once the mass is determined at the inlet, the mass flow rate (plus the overspary mass) maintains constant throughout the entire compressor, and the volume flow rate will change at different stages.
2. The mean diameter was designed the same for all the stages.
3. All the losses are assumed to occur in the rotor. There is no loss in stator, and the stator is assumed adiabatic (i.e. isentropic), so the total property values are the same at the inlet and exit of stators.
4. Property values (e.g. density, enthalpy) of mixture are calculated by mass-weighted average method, similar to the process described by Young [27].
5. Equation of state holds true for all conditions.
6. The system is assumed in thermodynamic equilibrium for droplet evaporation, i.e. water evaporation is governed by only thermodynamics per saturation requirement in each stage, although in reality, water evaporation is also governed by heat and mass transfer.
7. The water droplets are assumed incompressible, so the multi-phase flow can be represented by the polytropic process of moist air (dry air plus water vapor) with an equivalent polytropic index, k, as shown in Eq. (8). Keppler et al. [26] showed that k is approximately 1.36 for a wide range of air water mixture.

Numerical Procedure in Details

1. Provide the blade geometry (Tip Diameter – D_t, Hub Diameter - D_h, Hub-tip ratio and Cross-sectional area of flow passage– A).
2. Provide Ambient Temperature (T_{amb}), Pressure ($P_{amb} = P_1$), Relative Humidity (RH), Inlet Axial Velocity (V_{a1}), RPM (N), Water mass flow rate sprayed in each stage (if any).
3. Calculate inlet air psychrometric condition (ω_0, ω_1). If water is sprayed, calculate if saturation is reached before entering the compressor. If saturation is reached, calculate how much water vaporizes and how much water will enter the compressor in the liquid form. On the basis of calculated psychrometric condition, the static temperature in the first stage is determined. If air is saturated and/or oversprayed, the temperature is set at the wet bulb temperature (WBT); if air is not saturated, the temperature is calculated using the energy balance of a mixture.
4. Calculates total amount of water in each stage on the basis of upstream condition and the inter-stage spray in each stage.
5. Density (ρ_1) is calculated on the basis of static temperature (T_1) and static pressure (P_1) from Eq. (11).

$$\rho_1 = \rho_1(T_1, P_1) = \frac{1 + f_1 + g_1 + s_1}{\frac{1 + g_1}{\rho_m} + f_1 v_1 + s_1 v_s} \quad (11)$$

Where, f_1 = mass fraction of liquid water for P_1 and T_1.

g_1 = mass fraction of water vapor for P_1 and T_1.

v_1 = liquid water specific volume at P_1 and T_1. (From Steam Table)

v_s = Superheated steam specific volume at P_1 & T_1. (From Steam Table)

ρ_m = Mixture density of air and water vapor = $P_1/(R_m T_1)$

R_m = Gas constant for air and water vapor mixture = R_0/M_m.

R_0 = Universal gas constant = 8.314 kJ/kmole-K

M_m = Molecular weight of air and water vapor mixture

$= (28.965+18g_{1.5})/(1+g_{1.5})$

f_1 and g_1 are calculated from psychrometry. For T_1, saturation pressure (P_{sat}) is determined from the steam table. The total water per unit dry air required to reach saturation is ω_1, which is calculated from Eq. (12).

$$\omega_1 = \frac{0.622 P_{sat}}{P_1 - P_{sat}} \quad (12)$$

If ω_1 is larger than or equal to total amount of water in the current stage, the air will not reach saturation; then,

g_1 = Total amount of water in stage 1, and $f_1 = 0$

otherwise,

$g_1 = \omega_1$, and f_1 = Total amount of water in stage 1 – g_1.

If P_{sat} is larger than P_1, the water vapor is superheated and whole amount of water is superheated, which means there is no liquid water or saturated steam (i.e. $f_1 = g_1 = 0$).

6. Mass flow rate (m_1) is calculated out from mass conservation (Eq. 13).

$$\dot{m}_1 = \rho_1 A_1 V_1 \quad (13)$$

7. The mass flow rate from Eq. (13) remains constant throughout the process unless there is any further interstage spray in downstream stage(s). If there is spray in other stage(s), based on the amount of water in each stage, flow rate in each stage is updated.

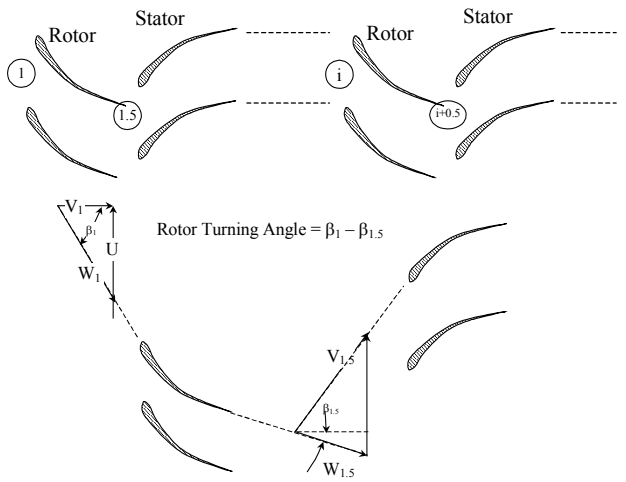

Figure 2 Rotor-Stator Staging

First Stage Rotor Inlet (Stage 1 in Fig. 2):

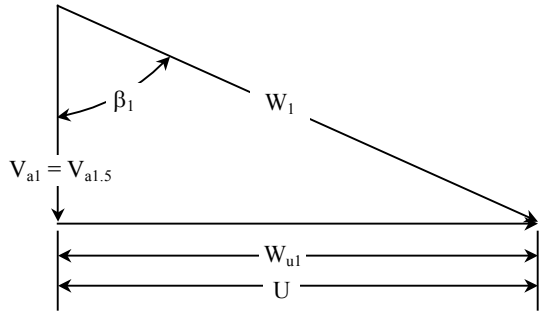

Figure 3 Velocity Diagram

8. Rotor inlet velocity is assumed coming in as a pure axial velocity (i.e. V1 = V_{a1}) without the tangential component. The relative velocity (W_1) is calculated from the velocity diagram (Fig. 3) with the known tangential velocity U = N x r. Axial velocity remains the same for stator (i.e. $V_{a1} = V_{a1.5}$),for the design case, but the axial velocity changes for other cases.

9. Moist air static enthalpy (h_1) is calculated from Eq. (14).

$$h_1 = h_1(T_1, P_1) = \frac{h_{a_1} + f_1 h_{f_1} + g_1 h_{g_1} + s_1 h_{s_1}}{1 + f_1 + g_1 + s_1} \quad (14)$$

Where, h_{a1} = dry air enthalpy at T_1. (From air property table)

h_{f1} = liquid water enthalpy at P_1 and T_1. (From steam table)

h_{g1} = saturated vapor water enthalpy at T_1. (From steam table)

h_{s1} = superheated steam enthalpy at P_1 and T_1. (From steam table)

s_1 = mass fraction of superheated steam for P_1 and T_1.

f_1, g_1 and s_1 are calculated from Eq. (12) shown in step 5.

10. The total enthalpy (ho_1) for rotor is calculated from Eq. (15).

$$ho_1 = h_1 + \tfrac{1}{2} V_1^2 \quad (15)$$

11. The total temperature (To_1) and total pressure (Po_1) for rotor are determined by iteration:
    (a) Guess a total temperature (To_1) and calculate the total pressure (Po_1) from Eq. (16) using equivalent polytropic index for moist air.

$$\frac{Po_1}{P_1} = \left(\frac{To_1}{T_1}\right)^{\frac{k}{k-1}} \quad (16)$$

    (b) Determine the total enthalpies of all phases with guessed total temperature (To_1) and total pressure (Po_1). Moist air total enthalpy (ho_1) is calculated from Eq. (17).

$$ho_1 = ho_1(To_1, Po_1) = \frac{h_{a_1} + f_1 ho_{f_1} + g_1 ho_{g_1} + s_1 ho_{s_1}}{1 + f_1 + g_1 + s_1} \quad (17)$$

    f_1, g_1 & s_1 are calculated from Eq. (12) shown in step 5.

    (c) Determine the moist air total enthalpy from Eq. (17) and compare it with the calculated total enthalpy from Eq. (15). Repeat step (a) to (c) until convergence.

First Stage Rotor Exit or Stator Inlet (Stage 1.5 in Fig. 2):

12. Determine the relative velocity angle ($\beta_{1.5}$) from β_1, mass flow rate for water spray (if any), and rotor turning angle (θ) with Eq. (19) by assuming the velocity follows the rotor surface contour and exits the rotor without deviating from the tangent of the camber line (i.e. the flow angles are the same as camber angles). The rotor turning angle (i.e. camber angle), θ, is known from the design blade geometry.

$$\beta_{1.5} = \beta_1 + \theta \quad (19)$$

13. Axial velocity ($Va_{1.5}$) at rotor exit is determined by iteration:

    (a) Guess a rotor exit velocity ($Va_{1.5}$).

    (b) Determine the other velocity components at the rotor exit from the tentative velocity diagram (Fig. 4)

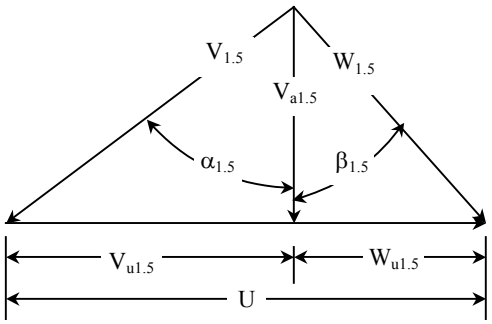

Figure 4 Velocity Diagram at rotor exit

    (c) The specific isentropic work imposed on the rotor is calculated from :

$$\text{Work}_S = U(Vu_1 - Vu_{1.5}) \quad (20)$$

Since the flow is assumed to turn exactly the same angle as the camber turning angle, the work produced is therefore the ideal (isentropic) work. Because in the real process, the friction in the boundary layer or secondary flow will affect the flow angle and requires more compressor work. The flow will leave the trailing edge with a deviation angle.

(d) Determine the total enthalpy at rotor exit as:

$$ho_{1.5} = ho_1 - \text{Work}_S/\eta_S \quad (21)$$

where, η_S is the stage isentropic efficiency.

(e) The total temperature ($To_{1.5}$) and the total pressure ($Po_{1.5}$) at rotor exit is determined by iteration:

(i) Guess a total temperature ($To_{1.5}$) and calculate total pressure ($Po_{1.5}$) from:

$$\frac{Po_{1.5}}{Po_1} = \left(\frac{To_{1.5}}{To_1}\right)^{\frac{k\eta_S}{(k-1)}} \quad (22)$$

Note that stage isentropic efficiency, η_s, is used here instead of small-stage efficiency, η_p, because the calculation is cross over the entire stage instead of an infinitesimal small element.

(ii) Determine the total enthalpies of all phases with the guessed temperature ($To_{1.5}$) and the calculated total pressure ($Po_{1.5}$) from Eq. (22). Moist air total enthalpy ($ho_{1.5}$) is calculated from Eq. (17) by changing the subscript from 1 to 1.5.

(f) Calculate the static enthalpy ($h_{1.5}$) from Eq. (23).

$$h_{1.5} = ho_{1.5} - \tfrac{1}{2}V_{1.5}^2 \quad (23)$$

(g) Determine the rotor exit static temperature ($T_{1.5}$) and static pressure ($P_{1.5}$) by iteration:

(i) Guess a static temperature and calculate static pressure by Eq. (16) by changing the subscripts from 1 to 1.5.

(ii) Determine enthalpies of all phases with guessed temperature ($T_{1.5}$) and the calculated static pressure ($P_{1.5}$) from Eq. (16). Moist air static enthalpy ($h_{1.5}$) is calculated from Eq. (14) by changing subscripts from 1 to 1.5.

(iii) Calculate the moist air static enthalpy from Eq. (14) and compare it with the calculated static enthalpy from Eq. (23). Repeat step (i) to (ii) until convergence.

(j) Density ($\rho_{1.5}$) is calculated from Eq. (11) on the basis of static temperature ($T_{1.5}$) and static pressure ($P_{1.5}$) shown in step 5.

(k) Calculate the mass flow rate from Eq. (24).

$$\dot{m}_{1.5} = \rho_{1.5} A_{1.5} Va_{1.5} \quad (24)$$

(l) Compare the mass flow rate from Eq. (24) with that from step 12 and repeat step (a) to (k) until convergence.

14. Determine the other velocity component at rotor exit from the velocity diagram (Fig. 4)

15. Torque, power and work are calculated from Eqs. (25), (26) & (20).

$$\text{Torque}_1 = \dot{m}\frac{D}{2}(Vu_1 - Vu_{1.5}) \quad (25)$$

$$\text{Power}_1 = \text{Torque} \times \frac{2\pi N}{60} \quad (26)$$

16. Determine the total enthalpy at rotor exit from Eq. (21).

17. At this point, although the total temperature ($To_{1.5}$) and total pressure ($Po_{1.5}$) at the rotor exit has been calculated in step 13(e), they need to be updated with the correct axial velocity obtained by Eq. 24 in step 13(k). Therefore, the total temperature ($To_{1.5}$) and total pressure ($Po_{1.5}$) at rotor exit needs to be determined again by iteration:

(a) Guess a total temperature ($To_{1.5}$) and calculate total pressure ($Po_{1.5}$) from Eq. (16) by changing subscripts from 1 to 1.5.

(b) Determine the total enthalpies of all phases with guessed temperature ($To_{1.5}$) and the calculated total pressure ($Po_{1.5}$) from step (a). Moist air total enthalpy ($ho_{1.5}$) is calculated from Eq. (17) by changing subscripts from 1 to 1.5.

(c) Compare the total enthalpy from step 17(b) with calculated total enthalpy from step 16 and repeat step (a) to (c) until convergence.

18. Calculate the static enthalpy ($h_{1.5}$) at rotor exit from Eq. (23).

19. Determine the static temperature ($T_{1.5}$) and static pressure ($P_{1.5}$) at rotor exit by iteration:

(a) Guess a static temperature and calculate static pressure by Eq. (26) by changing subscripts from 1 to 1.5.

(b) Determine static enthalpies of all phases with guessed temperature ($T_{1.5}$) and calculated static pressure ($P_{1.5}$). Moist air static enthalpy ($h_{1.5}$) is calculated from Eq. (14) by changing subscripts from 1 to 1.5.

(c) Compare the moist air static enthalpy from step 19(b) with the calculated enthalpy from step 18 and repeat step (a) to (b) until convergence.

20. Density ($\rho_{1.5}$) is calculated on the basis of static temperature ($T_{1.5}$) and static pressure ($P_{1.5}$) from equation shown in step 5.

Other Stage Rotor Inlets (Stage i in Fig. 2):

21. If water is sprayed at the previous stator stage (Stage i-0.5), calculate if saturation is reached before exiting the previous stator stage. If saturation is reached, calculate how much water vaporizes, and how much water will enter the compressor in the

liquid form. Calculate air psychrometric condition (ω_0, ω_1) at the rotor inlet (Stage i). On the basis of calculated psychrometric condition, the static temperature at the Stage i rotor inlet is determined. If air is saturated and/or oversprayed, the temperature is set at the WBT; if air is not saturated, the temperature is calculated using the energy balance of a mixture.

22. Update the mass fractions of all components, f_i, g_i, and s_i.

21. Since no heat or frictional loss are assumed over the stator stage, at the inlet of rotor stage i, the total pressure ($Po_i = Po_{i-0.5}$), total temperature ($To_i = To_{i-0.5}$), total enthalpy ($ho_i = ho_{i-0.5}$) and inlet velocity angle ($\alpha_i = \alpha_{i-0.5}$ - stator turning angle) are calculated from the previous stator inlet.

22. Static temperature, static pressure and inlet velocity and axial velocity at rotor inlet are iterated:

    (a) Guess a static temperature (T_i) and calculate static pressure (P_i) by Eq. (16) by changing subscripts from 1 to i.

    (b) Determine the static enthalpies of all phases with guessed temperature (T_i) and the calculated static pressure (P_i) from Eq. (16). Moist air static enthalpy (h_i) is calculated from Eq. (14) by changing subscripts from 1 to i.

    (c) Density (ρ_i) is calculated on the basis of static temperature (T_i) and static pressure (P_i) from Eq. (11) shown in step 5.

    (d) Calculate the rotor inlet velocity (V_i) from Eq. (27).

$$h_i = ho_i - \tfrac{1}{2} V_i^2 \quad (27)$$

    (e) Calculate the axial velocity (Va_i) from Eq. (28).

$$Va_i = V_i \mathrm{Cos}(\alpha_i) \quad (28)$$

    (f) Find the flow rate (m_i) from Eq. (29).

$$\dot{m}_i = \rho_i A_i Va_i \quad (29)$$

    Compare this value with the flow rate calculated from Eq. (13) and repeat step (a) to (f) until convergence.

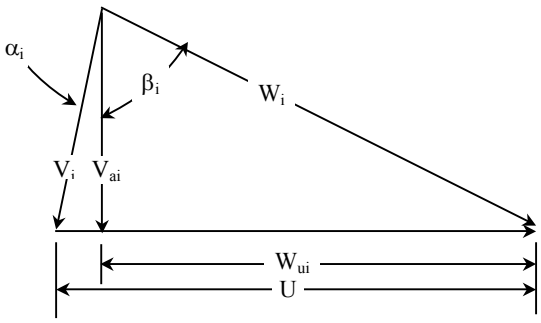

Figure 5 Velocity Diagram at rotor inlet

23. Determine the other velocity components at rotor inlet from the velocity diagram Fig. 5. Find the static enthalpy from Eq. (14) by changing subscripts from 1 to i.

24. Density (ρ_i) is calculated on the basis of static temperature (T_i) and static pressure (P_i) from Eq. (11) as shown in step 5.

25. Find the other velocities for the stator from velocity diagram (Fig. 5)

Other Stage Rotor Exits or Stator Inlets (Stage i+0.5 in Fig. 2):

(26) Repeat step 12 to step 20.

The algorithm is written in Access and incorporated in FogGT. A case study is performed in Part 2 of this paper [28].

SUMMARY

A wet compression thermodynamic model for fogging, overspray, and interstage spray has been developed using the stage-stacking scheme including the analysis of the pre-heat and pre-cool effect at each small stage of the overall compressor performance. An algorithm has been developed to calculate the local velocity diagram by allowing a stage-by-stage analysis of the fogging effect on airfoil aerodynamics and loading with known 2-D meanline rotor and stator geometries. Thermal equilibrium model for water droplet evaporation is adopted. The stage-stacking scheme is straightforward for the design case computation, but it becomes burdensome for off-design cases with wet compression in hot and dry weather. Furthermore, aerodynamic analysis makes the computation more complicated. Iterations are conducted to ensure the specific stage work obtained from the velocity diagram matches the total enthalpy increase obtained from the polytropic relationship (i.e. aerodynamics results must match the thermodynamic results.) The developed theory and algorithm are integrated into the system-wise FogGT program for calculating the overall gas turbine system performance.

ACKNOWLEDGEMENT

This study was supported by the Louisiana Governor's Energy Initiative via the Clean Power and Energy Research Consortium (CPERC) and administered by the Louisiana Board of Regents.

REFERENCES

1. Meher-Homji, C.B. and Mee, T.R., 1999, "Gas Turbine Power Augmentation by Fogging of Inlet Air", Proceedings of 28th Turbomachinery Symposium, Houston, Texas, USA, September 1999.
2. Bagnoli, M., Bianchi, M., Melino, F., Peretto, A., Spina, P.R., Bhargava, R. and Ingistov S., 2004, "A Parametric Study of Interstage Injection on GE Frame 7EA Gas Turbine", Proceedings of ASME Turbo Expo 2004, Vienna, Austria, June 14-17, ASME Paper No: GT-2004-53042.
3. Ingistov, S., 2001, "Interstage Injection System for Heavy Duty Industrial Gas Turbine Model 7EA," ASME Paper 2001-GT-407, Turbo Expo2001, New Orleans
4. Shepherd, D. W. and Fraser, D., 2006, "Impact of Heat Rate, Emissions and Reliability from the Application of Wet Compression on Combustion Turbines", Power-Gen International, Las Vegas, Nevada, USA, Nov 28-30, 2006.
5. Hill P. G., "Aerodynamic and Thermodynamic Effects of Coolant Injection on Axial Compressors", Aeronautical Quarterly, February 1963, pp. 333-348.
6. Zheng, Q., Sun, Y., Li, S. and Wang, Y, 2002, "Thermodynamic Analysis of Wet Compression Process in the Compressor of Gas Turbine", Proc. of ASME Turbo Expo 2002, Amsterdam, The Netherlands, June 3-6, ASME Paper No: GT-2002-30590.

7. Zheng, Q., Li, M., Sun, Y., 2003, “Thermodynamic Analysis of Wet Compression and Regenerative (WCR) Gas Turbine”, Proceedings of ASME Turbo Expo 2003, Atlanta, Georgia, USA, June 16-19, ASME Paper No: GT-2003-38517.
8. Ransom, D., Brun, K. and Kurz, R., 2007, “Enthalpy Determination Methods for Compressor Performance Calculations”, Proceedings of ASME Turbo Expo 2007, Montreal, Canada, May 14-17, 2007, ASME Paper No: GT-2007-27038.
9. Li, M. and Zheng, Q., 2004, “Wet Compression System Stability Analysis”, Proceedings of ASME Turbo Expo 2004, Vienna, Austria, June 14-17, 2004, ASME Paper No: GT-2004-54018.
10. Roumeliotis I., Mathioudakis K., 2006, “Evaluation of Interstage Water Injection Effect on Compressor and Engine Performance”, ASME Journal of Engineering for Gas Turbine and Power, Paper GTP-05-1123, Vol. 128/4, pp. 849-856, Also ASME paper 2005-GT-68698.
11. Lecheler S., Hoffman J., 2003, “The Power of Water in Gas Turbines: ALSTOM’s Experience with Air Inlet Cooling”, Proc. PowerGen 2003 São Paolo, Brasil, Nov. 11-13.
12. Payne, R.C. and White, A.J., 2007, “Three-Dimensional Calculations of Evaporative Flow in Compressor Blade Rows”, Proceedings of ASME Turbo Expo 2007, Montreal, Canada, May 14-17, 2007, ASME Paper No: GT-2007-27331.
13. Bagnoli, M., Bianchi, M., Melino, F. and Spina, P.R., 2006, “Development and Validation of a Computational Code for Wet Compression Simulation of Gas Turbines”, Proceedings of ASME Turbo Expo 2006, Barcelona, Spain, May 8-11, 2006, ASME Paper No: GT-2006-90342.
14. Bagnoli, M., Bianchi, M., Melino, F., Peretto, A., Spina, P.R., Ingistov S. and Bhargava, R.K., 2006, “Application of a Computational Code to Simulate Interstage Injection Effects on GE Frame 7EA Gas Turbine”, Proceedings of ASME Turbo Expo 2006, Barcelona, Spain, May 8-11, 2006, ASME Paper No: GT-2006-90343.
15. White A. J., Meacock A. J., 2004, “An Evaluation of the Effects of Water Injection on Compressor Performance”, ASME J. of Engineering for Gas Turbines and Power, Vol. 126, pp.748-754.
16. Abdelwahab, A., 2006, “An Investigation Of The Use Of Wet Compression In Industrial Centrifugal Compressors”, Proceedings of ASME Turbo Expo 2006, Barcelona, Spain, May 8-11, 2006, ASME Paper No: GT-2006-90695.
17. Zamzam, M.M. and Al-Amiri, A.M., 2007, “A Novel Free-cooling Scheme for Combustion Turbine Inlet Air Cooling”, Proceedings of ASME Turbo Expo 2007, Montreal, Canada, May 14-17, 2007, ASME Paper No: GT-2007-27621.
18. Sanaye, S., Rezazadeh, H. and Aghazeynali, M., 2006, “Effects of Inlet Fogging and Wet Compression on Gas Turbine Performance”, Proceedings of ASME Turbo Expo 2006, Barcelona, Spain, May 8-11, 2006, ASME Paper No: GT-2006-90719.
19. Spina, P. R., 2002, “Gas Turbine Performance Prediction by using Generalized Performance Curves of Compressor and Turbine Stages”, Proceedings of ASME Turbo Expo 2002, Amsterdam, The Netherlands, June 3-6, 2002, ASME Paper No: GT-2002-30275.
20. Bianchi, M., Melino, F., Peretto, A., Spina, P.R. and Ingistov S., 2007, “Influence of Water Droplet Size and Temperature on Wet Compression”, Proceedings of ASME Turbo Expo 2007, Montreal, Canada, May 14-17, 2007, ASME Paper No: GT-2007-27458.
21. Sexton, M. R., Urbach, H. B., Knauss, D. T., 1998 “Evaporative Cooling for NOx Suppression and Enhanced Engine Performance for Naval Gas Turbine Propulsion Plants”, ASME paper 98-GT-332.
22. Kim, K. H. and Perez-Blanco, H., 2006, “An Assessment of High-Fogging Potential for Enhanced Compressor Performance”, Proceedings of ASME Turbo Expo 2006, Barcelona, Spain, May 8-11, 2006, ASME Paper No: GT-2006-90482.
23. Khan, J. R. and Wang, T., 2006, “Fog and Overspray Cooling for Gas Turbine Systems with Low Calorific Value Fuels”, Proceedings of ASME Turbo Expo 2006, Barcelona, Spain, May 8-11, 2006, ASME Paper No: GT-2006-90396.
24. Saravanamuttoo, H. I. H., Cohen, H. and Rogers, G. 1996, Gas Turbine Theory, 4th Ed., Longman, 1996.
25. Wilson, D. G. and Korakianitis, T., 1988, " The Design of High-Efficiency Turbomachinery and Gas Turbines," Prentice Hall, 2nd ed. pp.79 -87.
26. Klepper J., Hale A., Davis M., Hurwitz W., “A Numerical Investigation of the Effects of Steam Ingestion on Compression System Performance”, ASME paper No. GT2004-54190.
27. Young J. B., “The Fundamental Equations of Gas-Droplet Multiphase Flow”, Int. J. Multiphase Flow, Vol. 21, No. 2, pp.175-191, 1995.
28. Wang, T. and Khan, J. R., 2008, " Overspray and Interstage Fog Cooling in Compressor using Stage-Stacking Scheme - Part 2: Case Study," ASME Paper GT2008-50323, ASME Turbo Expo2008, Berlin, Germany, June 9-13, 2008.

APPENDIX

Chart 1 Flow chart for simulation (for rotor and stator from second stage)